Check for updates

RESEARCH ARTICLE

ADVANCED OPTICAL MATERIALS
www.advopticalmat.de

Liquid Crystal 3D Optical Waveguides Based on Photoalignment

*Peter Ropač, Yu-Tung Hsiao, Brecht Berteloot, Yera Ussembayev, Inge Nys, Miha Ravnik, and Kristiaan Neyts**

A novel design and approach for the realization of liquid crystal optical waveguides using photopatterning as a manufacturing method is presented. The developed method is used to demonstrate straight waveguides of different widths and curved waveguides with different radius of curvature. The waveguides are terminated with +1 or −1 surface defects through which the light incouples/outcouples. The effect of the straight waveguide thickness and the radius of curvature of the curved waveguides on the attenuation of the light in the waveguide is experimentally explored. The experiments are supported with numerical simulations of light propagation through both types of waveguides and outcoupling out of the straight waveguides. Furthermore, the effect of the size of the −1 defect terminations on the outcoupling efficiency is explored using simulations. Based on the presented design and manufacturing approach, liquid crystal optical waveguides of various shapes can be realized accurately with low-cost.

P. Ropač, M. Ravnik
Faculty of Mathematics and Physics
University of Ljubljana
Jadranska ulica 19, Ljubljana 1000, Slovenia

P. Ropač, M. Ravnik
Jožef Stefan Institute
Jamova cesta 39, Ljubljana 1000, Slovenia

Y.-T. Hsiao, B. Berteloot, Y. Ussembayev, I. Nys, K. Neyts
ELIS Department
Ghent University
Technologiepark-Zwijnaarde 126, Ghent 9052, Belgium
E-mail: eeneyts@ust.hk

M. Ravnik
International Institute for Sustainability with Knotted Chiral Meta Matter
2–313 Kagamiyama, Hiroshima 739-0046, Japan

K. Neyts
Department of Electronic and Computer Engineering
The Hong Kong University of Science and Technology
Clear Water Bay, Kowloon, Hong Kong, SAR, Hong Kong

K. Neyts
State Key Laboratory of Advanced Displays and Optoelectronics Technologies
Clear Water Bay, Kowloon, Hong Kong, SAR, Hong Kong

The ORCID identification number(s) for the author(s) of this article can be found under https://doi.org/10.1002/adom.202402174

© 2024 The Author(s). Advanced Optical Materials published by Wiley-VCH GmbH. This is an open access article under the terms of the Creative Commons Attribution-NonCommercial License, which permits use, distribution and reproduction in any medium, provided the original work is properly cited and is not used for commercial purposes.

DOI: 10.1002/adom.202402174

1. Introduction

Optical waveguides are essential for tele- and data communication technology, serving as transportation channels for high-frequency signals with the speed of light. Optical glass fibers with very low loss in the telecom C-band are used for intercontinental fiber networks, while plastic optical fibers are used for smaller scale networks. In silicon photonics, the refractive index contrast is very high, and curved waveguides with a small radius of curvature are possible. In all these waveguide platforms, the propagation of light is realized efficiently, but for modulation and routing, hybrid integration with other material systems is often necessary.[1–3]

Nematic liquid crystals (LCs) are uniaxial soft materials with anisotropic properties, which self-organize by minimizing the elastic free energy for given boundary conditions. Under the influence of a small applied voltage, the optical axis can reorient, and this can be used to add a switching or modulation functionality to an optical device. Different approaches for the integration of LC with optical waveguides have been proposed.[4] In one approach, LC is infiltrated in one or more microcapillary cavities present in an optical glass fiber. By applying a potential difference between two electrodes at both sides of the fiber, the LC can reorient and influence the transmission characteristic of the fiber.[5–7] Another approach uses LC as a cladding for silicon on insulator waveguides. Reorientation of the LC modifies the optical properties of the cladding and this can modify the resonance frequency of a ring resonator.[8–10] Sometimes, the LC forms the core of the optical waveguide, and the geometry of the environment is used to confine the waveguide.[11,12] Alternatively, a waveguide may be induced by the application of an applied ac voltage in a LC layer with homogeneous alignment, when one of the electrodes has the shape of a narrow line.[13] Instead of using an externally applied electric field, the optical beam itself can also be used to reorient the LC. This non-linear self-induced optical waveguiding called a soliton or nematicon, requires minimal laser power to achieve waveguiding.[13–15]

The principle of photoalignment for nematic LC has added a new toolbox for the design of LC devices. This technology is based on a thin layer of photosensitive materials, which obtains a preferential orientation under the influence of linearly polarized (usually blue or UV) light.[16] When nematic LC is deposited

 © 2024 The Author(s). Advanced Optical Materials published by Wiley-VCH GmbH

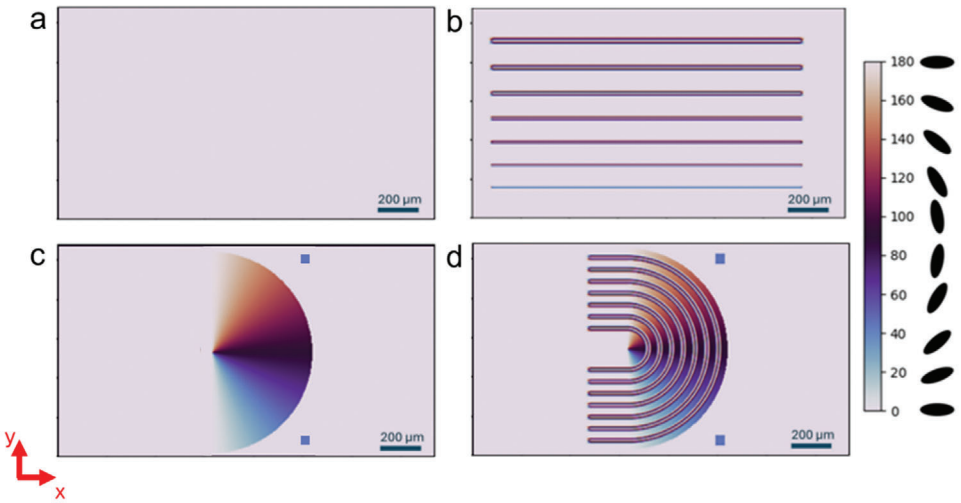

Figure 1. Alignment patterns for the waveguides. a) Bottom substrate alignment for straight waveguides; b) top substrate alignment for seven straight waveguides c) bottom substrate alignment for bent waveguides. d) Top substrate alignment for seven bent waveguides. The lavender background corresponds to horizontal alignment.

on top of this layer, the LC optical axis (also called the director) aligns with the preferential orientation. This approach has been used to create periodic diffraction gratings and different kinds of structures. Recently photoalignment has also been applied to create polymerized LC waveguides, in which the polymer forms the core of the waveguide and light is confined in one direction by the substrates and in the other direction by the orientation of the optical axis.[17,18]

Each of these approaches has its limitations when the aim is to realize waveguiding along variable paths, either because the LC is only modifying the phase of the light or because the waveguide path is fixed by the fabricated structure.

In this work we aim for an approach in which the waveguide path is completely within the LC layer and can be varied in two dimensions by the design of the photoalignment pattern: parallel to the substrate but also perpendicular to the substrate. This has the advantage that the liquid crystal orientation and the waveguide cross-section may further be influenced by the application of an external electric field. To demonstrate this approach, we design and fabricate LC optical waveguides by photoalignment in which the light is confined in two dimensions by the LC director orientation and verify the operation with experiments complemented by numerical modeling. In addition, we design incoupling and outcoupling sections at the ends of the waveguide, to bend the light toward one of the substrates.

2. Waveguide Design

The LC waveguide design is based on a central region with a high refractive index, combined with surroundings with a lower refractive index for a particular polarization. On the bottom substrate, the photoalignment direction is parallel to the direction of waveguiding (x-direction in **Figure 1**a). On the top substrate, away from the waveguide, the director follows the alignment at the bottom substrate, but above the waveguide, the alignment rotates in the XY plane over an angle of 360°, as illustrated in Figure 1b. The minimization of the elastic energy yields a director profile that aligns with the preferred orientation near the substrates (strong anchoring), with an alignment perpendicular to the substrates (along the z-axis) in the center of the waveguide. The vertical reorientation of the LC director in the bulk helps prevent the occurrence of twist disclinations caused by conflicting surface anchoring conditions at two substrates.[18] The lowest order waveguided mode is polarized with the electric field mainly perpendicular to the substrates (TM), parallel to the LC director in the central region.

The straight waveguides are terminated near the top substrate by a +1 defect at the left side in the photoalignment pattern and a −1 defect at the right side. The different sign of the two defects ensures that the waveguide is embedded in a region with homogeneous director orientation, parallel to the x-axis (see **Figure 2**a). The dimensions of the device are chosen as follows: the distance

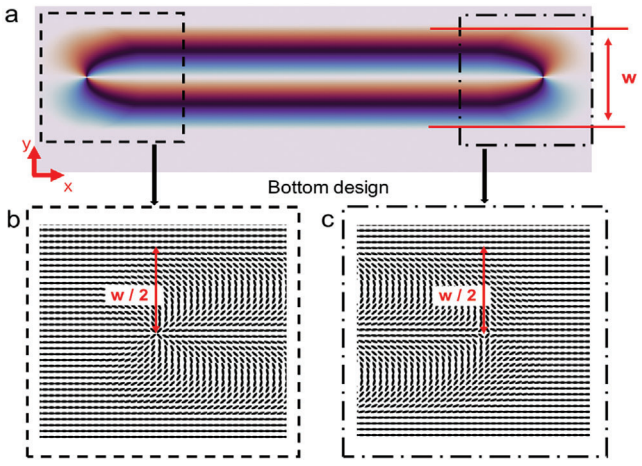

Figure 2. Alignment pattern at the top substrate for a shortened waveguide with width w, illustrating the alignment near the defects. a) Overall image of a shortened straight waveguide alignment pattern with b) S = +1 surface defect at the left end and c) S = −1 surface defect at the right end.

© 2024 The Author(s). Advanced Optical Materials published by Wiley-VCH GmbH

21951071, 2025, 4, Downloaded from https://advanced.onlinelibrary.wiley.com/doi/10.1002/adom.202402174 by Universiteitsbibliotheek Gent, Wiley Online Library on [18/03/2025]. See the Terms and Conditions (https://onlinelibrary.wiley.com/terms-and-conditions) on Wiley Online Library for rules of use; OA articles are governed by the applicable Creative Commons License

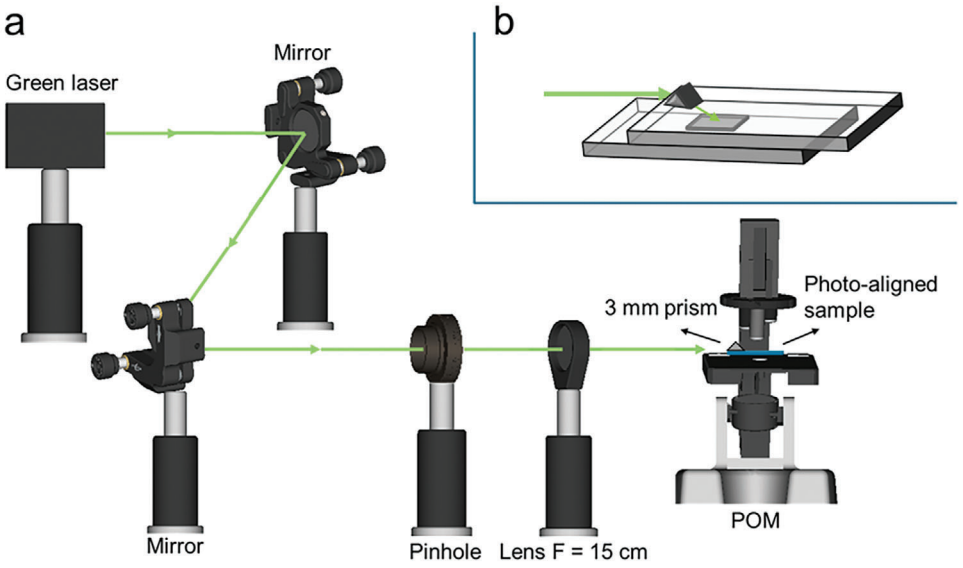

Figure 3. a) Measurement setup for incoupling of light in the LC waveguide, using a green laser, a lens, an incoupling prism and a polarization microscope. b) Inset illustrating the refraction of light by the prism and coupling to the photopatterned area in the sample.

between the two substrates is determined by the diameter of the spacers (5.5 µm). The width over which the director rotates over 360° is varied between 8 and 32 µm, and the length of the outcoupling section is equal to the width.

3. Results

3.1. Experimental Results

For the laser in-coupling into the LC waveguides, the setup illustrated in **Figure** 3a is built to achieve a large angle of incidence onto the top glass substrate while the device is observed with a polarized optical microscope. The 532 nm green laser beam is reflected by two mirrors to adjust and fine-tune the angle of incidence and the position of incidence into the LC layer. A lens with a focal distance of 150 mm, positioned at 150 mm before the substrate, is used to focus the laser beam onto the left end of the waveguide. A 45° prism with sides of 3 mm refracts the laser beam into the targeted waveguide with a large angle of incidence as illustrated in Figure 3b. We evaluate the waveguiding performance by observing light that is scattered out of the waveguide toward the objective of the polarizing optical microscope (POM). Under crossed polarizers, the reorientation of the LC director near the waveguides can be visualized.

The CCD camera attached to the polarization optical microscope (POM) with crossed polarizers can visualize the seven straight waveguides with different widths: 32, 28, 24, 20, 16, 12, and 8 µm (**Figure** 4a). By switching off the microscope illumination and switching on the green laser, the setup can visualize the light coupling into the straight waveguides and transport over a distance of 1240 µm to reach the right end of the waveguide, as shown for the waveguides with width 32 and 8 µm in Figure 4b,c. Note that the visualization with the microscope is based on the

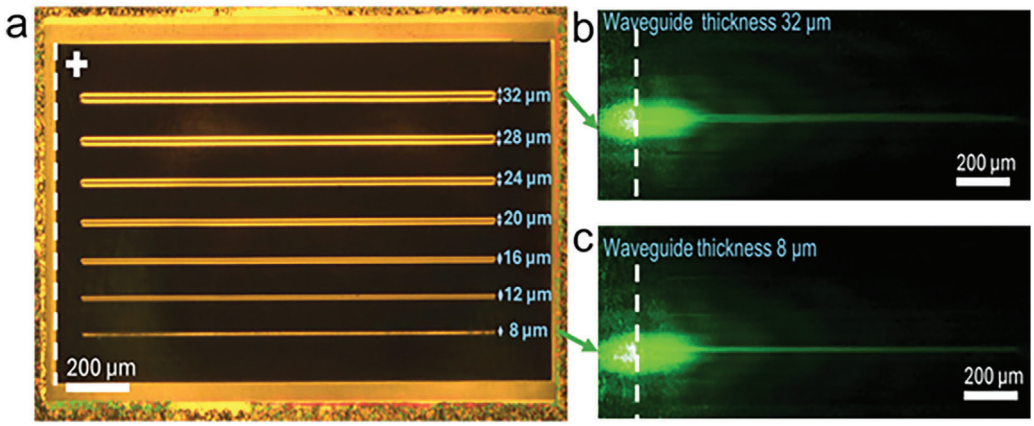

Figure 4. Microscope images of the waveguides. a) Seven straight waveguides obtained by patterned photoalignment, observed with POM with crossed polarizers, without laser light. b) Light coupling and waveguiding in the waveguide with width 32 µm. c) Light coupling and waveguiding in the waveguide with width 8 µm. The white dashed line indicates the edge of the photoaligned area.

© 2024 The Author(s). Advanced Optical Materials published by Wiley-VCH GmbH

21951071, 2025, 4, Downloaded from https://advanced.onlinelibrary.wiley.com/doi/10.1002/adom.202402174 by Universiteitsbibliotheek Gent, Wiley Online Library on [18/03/2025]. See the Terms and Conditions (https://onlinelibrary.wiley.com/terms-and-conditions) on Wiley Online Library for rules of use; OA articles are governed by the applicable Creative Commons License

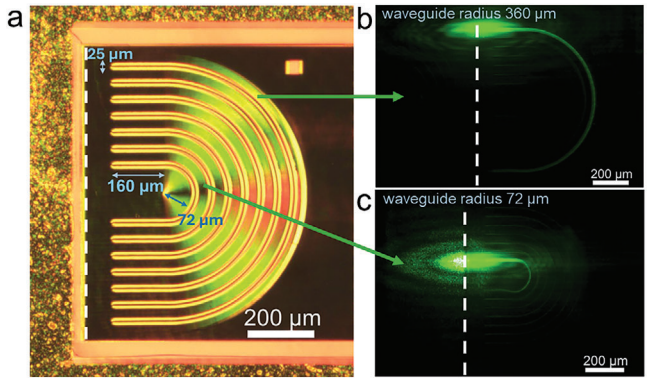

Figure 5. Microscope images of the bent waveguides. a) Seven bent waveguides created through patterned photoalignment, observed using POM with crossed polarizers, without the presence of laser light. b) Light coupling and waveguiding within the waveguide with a radius of 360 µm. c) Light coupling and waveguiding into the bent waveguide with a radius of 72 µm. The white dashed line indicates the edge of the photoaligned area.

light that is scattered out of the waveguide and captured by the objective of the microscope. The bright area near the left edge is due to scattering of the incident laser beam when it enters the LC layer.

Figure 5a shows the 7 waveguides that make a 180° curve in the POM with crossed polarizers. Each of the waveguides has a width of 25 µm and the radii vary from 72 to 360 µm. Note that in this case the background between the waveguides is bright, because the director in this area remains parallel with the waveguides and the LC layer acts as a retardation plate. In the middle of the curve, the background is reddish instead of dark, because the alignment is deviating from the design value and there is some twist in the layer. Figure 5a,b shows the incoupling region and waveguiding for the waveguides with the largest and smallest radius, when the green laser light is illuminating one end of the waveguide. The scattering at the incoupling section is similar as for the straight waveguides. In both cases, the waveguiding can be observed until the other end of the waveguide, while the intensity decreases along the path. It is obvious that the waveguide with the smallest radius (72 µm) has larger losses, and the region around the outer rim of the waveguide is also scattering light.

3.2. Numerical Simulations

Numerical simulations are done in three steps. In the first step, we calculate the bulk initial condition from the anchoring pattern on the top and bottom substrates using the open-source package for defining complex geometries SPOMSO.[19] With this approach, we can, in principle, calculate the bulk initial condition of an LC waveguide, which follows an arbitrary curve. In the second step, we determine the spatially dependent dielectric tensor by first calculating the director configuration by minimizing the Frank free energy, where we use the result of the previous step as the initial condition and the elastic energy constants of E7 LC k_{11} = 11.1 pN, k_{22} = 6.5 pN, k_{33} = 17.1 pN.[20] The resulting director configuration is converted into a spatially dependent dielectric tensor with ordinary and extraordinary refractive indices similar to those of E7, namely $n_e = 1.7558$ and $n_o = 1.5282$.[21] In the final step, the optics simulations are performed using the open-source package MEEP.[22] A continuous monochromatic multimode E_z (TM) polarized light source with a central wavelength of 532 nm is used.

With the above approach, we simulate the outcoupling of light through the −1 and +1 defect terminations of the straight waveguide with width w = 30 µm and cell thickness of 5.5 µm. Here we only show the results for the −1 termination since the outcoupling is analogous to the +1 defect termination. The simulation volume is centered around the center of the −1 defect. In **Figure 6**, we show the simulated director profile in different cross-sections for the −1 defect termination as well as the simulated propagation of light through the waveguide and the outcoupling into the glass substrate

In Figure 6c, a region can be observed, where the director is vertical (along the z-axis), and the effective refractive index is largest for the E_z polarization, forming the center of the effective waveguide for light from the multimode source. The light is waveguided in the region where the director is mostly vertical (Figure 6b), bends upward toward the −1 defect but fails to follow the imposed curvature of the waveguide (Figure 6e). As a result, the light does not efficiently outcouple into the top substrate at the location of the defect, but rather in the region after the defect (Figure 6b).

In **Figure 7**, we show the director configuration and light intensity profiles in different cross-sections for light traveling through a quarter-circle bent waveguide with radius 70 µm (for waveguide width 30 µm and cell thickness 5.5 µm). The director configuration in the cross-section along the width of the waveguide is the same as in the straight waveguide and similarly the light propagates in the region where the director is (almost) vertical before it enters the bent waveguide. The light exits the quarter circle waveguide more toward the outer edge of the waveguide cross-section. This is a consequence of the continuously varying refractive index, low contrast of the refractive indices, and the small radius of the quarter circle waveguide. Half/quarter circle waveguides with larger radii guide the light with less scattering (see Figure 4b). Additional simulations show that a significant amount of light is prematurely outcoupled through the top glass substrate.

Due to a continuously varying refractive index and a low contrast of refractive index in the waveguide, the light cannot follow the variation of the refractive index over a short length scale. Regardless of this fact, the propagation of light can still be improved. By controlling the size of the −1 defect termination along the x-axis (parameter u), the outcoupling efficiency can be improved by increasing the angle between the waveguided light and the substrate plane (see **Figure 8**). At $x = -u/2$ the orientation for the straight waveguide and for the −1 defect termination are connected. The size of the −1 defect termination is indicated by the dashed rectangle (see Figure 8a). As in Figure 6 the simulation volume is centered around the −1 defect. Figure 8a shows the director configuration for a −1 defect termination with u = 15 µm and u = 12 µm in the XZ plane at y = 0 µm. Figure 8b shows the propagation of light in the y = 0 µm plane (the same plane as in Figure 8a). As u decreases, the angle between the incident light and the substrate plane is increased, which increases the outcoupling efficiency, as in Figure 8c.

© 2024 The Author(s). Advanced Optical Materials published by Wiley-VCH GmbH

21951071, 2025, 4, Downloaded from https://advanced.onlinelibrary.wiley.com/doi/10.1002/adom.202402174 by Universiteitsbibliotheek Gent, Wiley Online Library on [18/03/2025]. See the Terms and Conditions (https://onlinelibrary.wiley.com/terms-and-conditions) on Wiley Online Library for rules of use; OA articles are governed by the applicable Creative Commons License

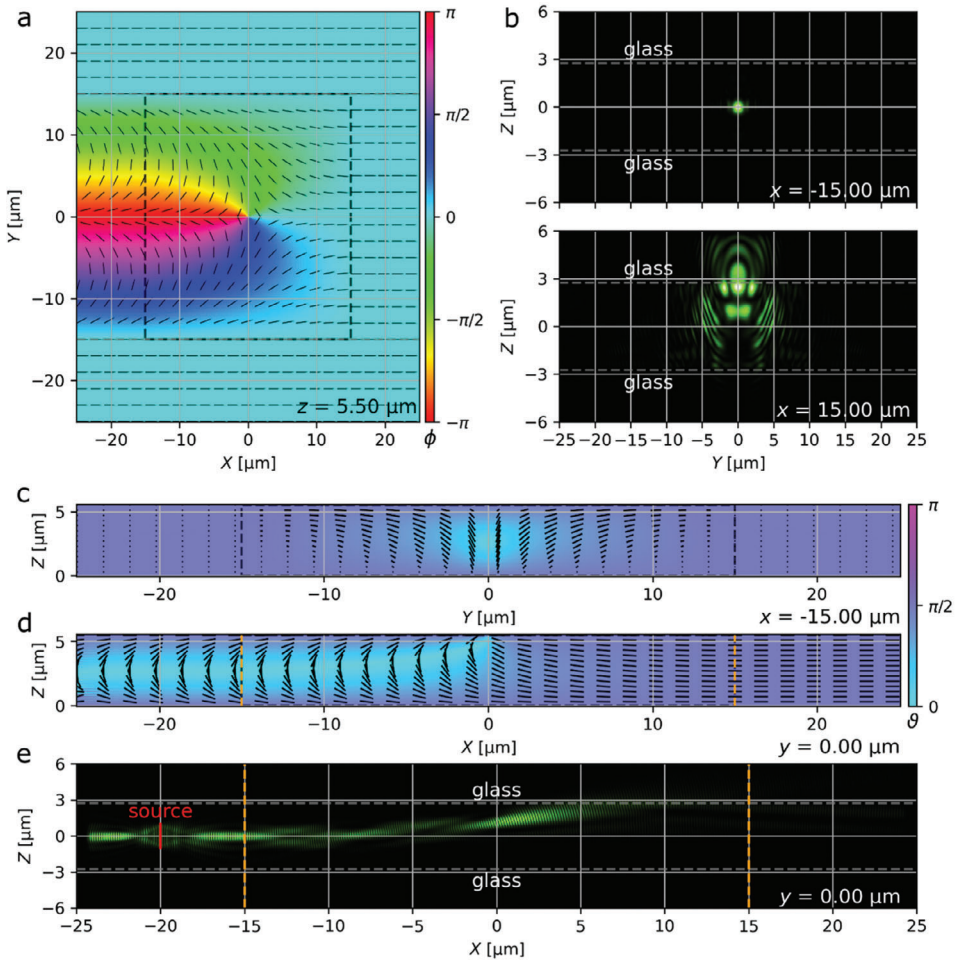

Figure 6. Director configuration and outcoupling of light near the −1 defect termination of the waveguide. The simulated waveguide width is w = 30 µm and the cell thickness is 5.5 µm. Director configurations at the substrate near the −1 defect in the XY plane a); in the YZ cross-section at x = −15 µm c); and in the YZ plane through the middle of the defect d). b) Intensity of light in the YZ cross-sections at x = −15 and +15 µm. e) XZ cross-section of light intensity through the middle of the waveguide (y = 0). Orange dashed lines mark the positions of the cross-sections from b). The maximum intensity of light in each of the slices is normalized to be equal to one.

4. Discussion

The experiments demonstrate that LC photoalignment patterning can effectively produce straight and half-circle optical waveguides. The experimental results are supported by numerical simulations of light propagation in three-dimensional anisotropic structures. In the experiments, light propagation along the waveguide is observed by imaging light that is scattered out of the waveguide toward the camera sensor. In the simulations, the propagation of electromagnetic waves along the waveguide and the losses out of the waveguide are computed. Dynamic short-range fluctuations in the director that can lead to large angle scattering of light toward the microscope objective are not included in the simulations.

In Figure 4, we demonstrate that the width w of the photoalignment pattern that defines the waveguide does not significantly affect the propagation distance, since for $w = 8$ and $w = 32$ µm, the light travels over the entire length of the waveguides (1240 µm). It should be noted that the region in which the light is concentrated (where the director is almost vertical, see Figure 6b) is much smaller than the width w of the photopatterned area. The area is much smaller because director configuration in the bulk relaxes to minimize the total elastic energy corresponding to the elastic constants of the LC and the anchoring patterns at the top and bottom substrates. The coupling of light into the waveguide is realized by a laser beam that makes a small angle with the substrate, which can excite many eigenmodes in the waveguide, particularly when the width of the waveguide is large.

With the half-circle curved LC waveguides (see Figure 5), we demonstrate that the waveguide design combined with photopatterning can be used to manufacture waveguides with different radius of curvature. From Figure 5b,c, it is evident that the scattering loss is larger for waveguides with a smaller radius of curvature. At the point where the curved section with 72 µm radius connects with the straight section of the waveguide, the path of the waveguided light deviates from the central region of the waveguide (as can be seen in Figure 5c). This effect is not observed for the waveguide with the 360 µm radius (see Figure 5b), which

© 2024 The Author(s). Advanced Optical Materials published by Wiley-VCH GmbH

21951071, 2025, 4, Downloaded from https://advanced.onlinelibrary.wiley.com/doi/10.1002/adom.202402174 by Universiteitsbibliotheek Gent, Wiley Online Library on [18/03/2025]. See the Terms and Conditions (https://onlinelibrary.wiley.com/terms-and-conditions) on Wiley Online Library for rules of use; OA articles are governed by the applicable Creative Commons License

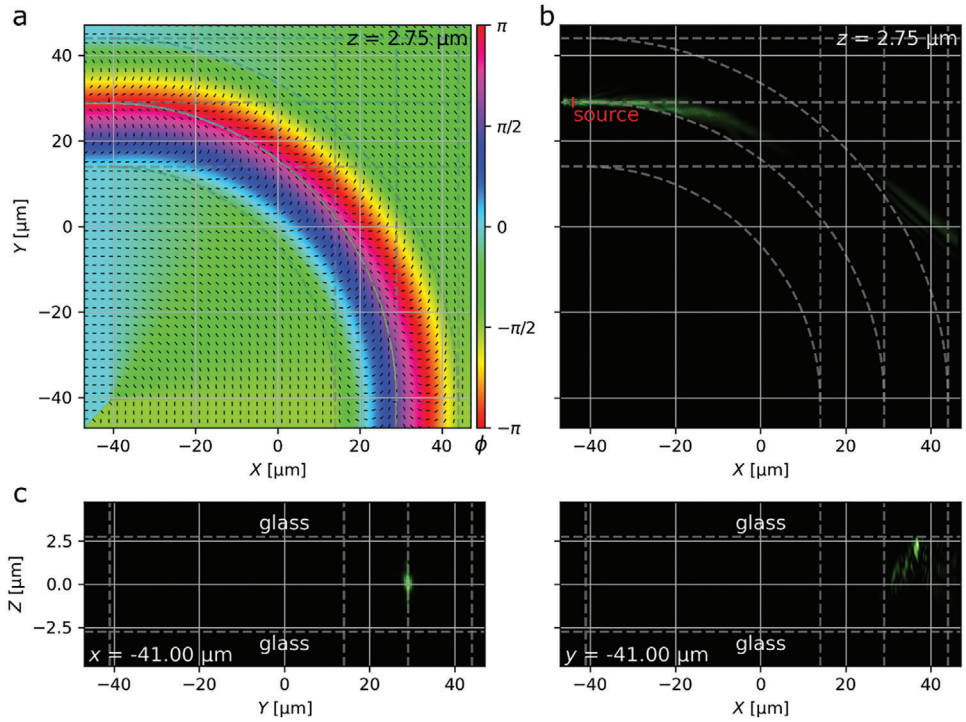

Figure 7. Director configuration and propagation of light in the quarter circle waveguide with the radius 70 μm and width 30 μm, in the cell with thickness 5.5 μm. a) director configuration at the top substrate. b) Propagation of light in the XY plane at half the thickness of the cell. c) Intensity profile near the source plane at x = −41 μm and at the end of the quarter circle waveguide at y = −41 μm. The maximum intensity of light in each of the slices is normalized to be equal to one.

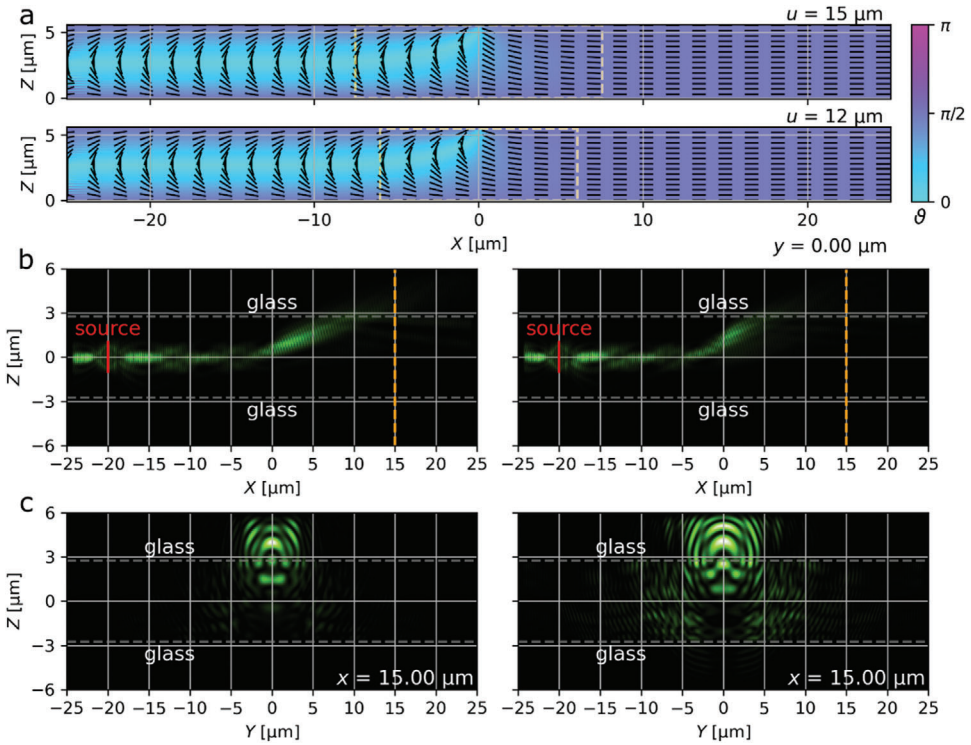

Figure 8. Director configurations and intensity profiles for straight waveguides with −1 defect termination with u = 15 μm and u = 12 μm. a) Director configuration in the XZ plane through the center of the −1 defect. b) Intensity profile in the same plane as in a). c) Intensity profiles in the YZ cross-section planes at x = 15 μm marked by the orange dashed lines in b). The maximum intensity of light in each of the slices is normalized to be equal to one.

© 2024 The Author(s). Advanced Optical Materials published by Wiley-VCH GmbH

21951071, 2025, 4, Downloaded from https://advanced.onlinelibrary.wiley.com/doi/10.1002/adom.202402174 by Universiteitsbibliotheek Gent, Wiley Online Library on [18/03/2025]. See the Terms and Conditions (https://onlinelibrary.wiley.com/terms-and-conditions) on Wiley Online Library for rules of use; OA articles are governed by the applicable Creative Commons License

indicates that the profile of the light in the waveguide cross-section is not everywhere the same. This experimental observation is supported by the numerical simulations shown in Figure 7c for the waveguide with radius of 70 µm. Figure 7b shows that if the radius of curvature is small, the light will no longer be localized in the center of the waveguide but rather scatter into regions with a slightly lower refractive index. Consequently, the profile of the light in the cross-section will be different where the light exits the curved section. Although it has been demonstrated that the design and manufacturing method allows to make a variety of waveguide circuits, further optimization of the waveguide trajectory may be considered to minimize scattering. One approach could be to implement a gradual change in the radius of curvature. The coupling loss from one waveguide section to another, as observed in Figure 5c, should be avoided. Figure 6 shows the simulated outcoupling of light from a straight waveguide section into the top glass substrate through a −1 defect waveguide termination. At $x = -15$ µm the director profile of the straight waveguide section starts transitioning into the director profile of the −1 defect at the top surface. Consequently, the region where the director is along the z-axis and the refractive index is the highest for E_z polarized light is curved upward toward the top substrate, and the light propagating in the waveguide follows a similar upward trajectory. As discussed previously, the propagating light cannot follow the center of the low-index contrast waveguide if the radius of curvature becomes too small. As a result, the light reaches the top substrate at a relatively small angle with the substrate, not at the location of the −1 defect (at $x = 0$ µm), but at a larger x-value. Since the light is incident at the top substrate at a shallow angle, and the substrate has a smaller refractive index than the LC, a large part of the incident light is reflected back into the LC cell (see Figure 6b,e). Another part of the light is transmitted into the substrate, but not as a Gaussian beam. According to reciprocity, the imperfect outcoupling of laser light from the waveguide into the glass substrate in the simulations indicates that the incoupling of laser light from the glass substrate into the waveguide will also be imperfect. This explains why the incoupling observed in the experiments of Figures 4b,c and 5b,c are not perfect, and only a fraction of the laser beam is coupled into the waveguide.

By reducing the region for the −1 defect termination in the x direction (parameter u), numerical simulations show that it is possible to increase the angle between the incident light and the substrate plane, and thereby also the outcoupling efficiency (see Figure 8b,c). While the electromagnetic wave does not follow the trajectory where the director has the z-orientation up to the −1 defect, the smaller radius of curvature induced by the smaller value of u, curves the light more toward the top substrate. Reducing u too much is not effective, because rapid variations of the director are limited by the elastic energy of the LC.

5. Conclusion

To conclude, a method based on photoalignment patterning to fabricate LC waveguides has been demonstrated. The waveguide path can be controlled in two dimensions, both parallel and perpendicular to the substrate. The incoupling of a laser beam and the light propagation in straight waveguides with different widths and curved waveguides with different radii of curvature was shown experimentally. The experimental results were interpreted in more detail based on numerical simulations, and the incoupling and outcoupling sections at the ends of the waveguide, that bend the light toward the top substrate, were studied. This approach has several advantages: the waveguide is completely embedded in the soft material; there is no loss due to absorption in electrodes that may be present at the surfaces; and the waveguide profile may be modified or shifted by the application of an electric field. In addition, the director at the surface may be modified because photoalignment can be rewritable.[23] Therefore, LC waveguide circuits with high complexity and low cost can be fabricated and used as building blocks in photonic circuits.

6. Experimental Section

Experiments: The preparation of devices with straight and curved waveguides requires the following steps. The two substrates (top and bottom substrates) are first thoroughly cleaned. Then a photoalignment layer, Brilliant Yellow, is deposited onto using spin-coating for 30 s at 3000 rpm with a solution composed of 0.2 wt % Brilliant Yellow in N,N-dimethylformamide. Subsequently, the coated substrates undergo a soft baking process at 90 °C for 5 min. A blue laser (Cobolt Twist $\lambda = 457$ nm) and a spatial light modulator (SLM, Holoeye Pluto 2, active area of 15.36 mm × 8.64 mm, resolution: 1920 × 1080 pixels) are used to create a polarization pattern with variable linear polarization by projecting the surface of the SLM onto an area of approximately 1.5 mm× 0.8 mm of the brilliant yellow layer, as illustrated in **Figure 9**. To achieve the designed patterns at two substrates, the desired retardation pattern on the SLM is programmed and translated into a digital driving level for the SLM, using an appropriate calibration procedure. By shifting the substrate between successive illuminations, straight and curved waveguide alignment patterns can be produced side by side on the respective top or bottom substrate. A detailed explanation of this setup is available in the following paper.[24,25]

Following the illumination during the photoalignment procedure, a thin layer of the reactive mesogen RM257 is applied through spin-coating at 1500 rpm for 30 s on each substrate. To achieve a thin layer, a 0.4wt% RM257 solution was prepared. This solution contains 0.4% RM257, 99.6% Toluene, along with a small quantity of photoinitiator (Irgacure 819) and inhibitor (tert-butylhydroquinone). After evaporation of the solvent, the LC

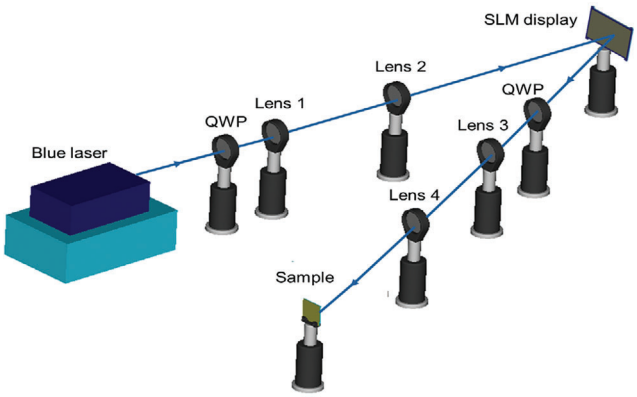

Figure 9. Spatial light modulator (SLM) setup used for photoalignment patterning. The linear polarization of the blue laser is transformed into circularly polarized light. The SLM modifies the retardation between the horizontal and vertical components. The second QWP generates linearly polarized light with spatially variable orientation.

© 2024 The Author(s). Advanced Optical Materials published by Wiley-VCH GmbH

21951071, 2025, 4, Downloaded from https://advanced.onlinelibrary.wiley.com/doi/10.1002/adom.202402174 by Universiteitsbibliotheek Gent, Wiley Online Library on [18/03/2025]. See the Terms and Conditions (https://onlinelibrary.wiley.com/terms-and-conditions) on Wiley Online Library for rules of use; OA articles are governed by the applicable Creative Commons License

layer undergoes polymerization under UV light for 5 min. Followed by polymerization, the photoalignment patterns become visible under the polarized optical microscope. Different patterns on the top and bottom substrates can be aligned more precisely by verifying the corresponding overlaps. Subsequently, the LC mixture E7 was filled into this assembled cell above the clearing temperature and slowly cooled to room temperature.

Simulations: The steps to simulate the propagation of light in the LC waveguides are the following. We define the shape of a waveguide using a photo editing software or a parametric function. With the Python package SPOMSO,[19] we calculate the signed distance function of the waveguide and compute the anchoring and bulk director configurations from the calculated signed distance function using our Ansatz. The resulting director configuration is the initial condition of the director configuration simulation based on Frank free energy. The minimization configuration software is proprietary and was developed to run heterogeneously on high performance CPUs and GPUs. The resulting director configuration is converted into spatially dependent dielectric tensor with ordinary and extraordinary refractive indices approximately matching those of E7 LC – n_e = 1.7558 and n_o = 1.5282.[21] In the final step, the optics simulations are performed using a finite-difference time-domain method implemented in the open-source package MEEP.[22] In the simulations, we use a multimode continuous E_z polarized source with a central wavelength of 532 nm, which is Gaussian in frequency space with the standard deviation being 0.2 times the central frequency. The simulations volume has a resolution of 30 points μm^{-1} and is surrounded with perfectly matched layers to absorb light scattered into the boundary of the simulation volume.

The size of the multimode source is determined by analyzing the sizes of the most prominent eigenmodes of the waveguide in different YZ plane cross-sections launched from a large source spanning the entire width and thickness of the waveguide. The size of the multimode source is such that the intensity in the source plane of the first eigenmode outside the area covered by the multimode source was less than 1% of its intensity at the center of the waveguide.

The simulations run until the light has fully propagated through the waveguides and a steady state is established. This is mostly a function of the waveguide length. For visualization, we export the electric and magnetic fields in different significant planar slices of the simulation volume. This approach allows us to design the anchoring patterns of arbitrarily shaped waveguide/waveguide networks, simulate the resulting director configuration in the bulk and simulate the propagation of light through the waveguide network.

Acknowledgements

P.R. and M.R. acknowledge funding from Slovenian Research Agency grants P1-0099, N1-0195, and J1-2462, and from the European Research Council (ERC) under the European Union's Horizon 2020 Research and Innovation Program (grant agreement no. 884928-LOGOS). Y.-T.H. was supported by a PhD Grant Strategic Basic Research of the Research Foundation-Flanders under Grant 1SHF924N. B.B. acknowledges funding by the Research Foundation-Flanders under grant 3G0C2121.

Conflict of Interest

The authors declare no conflict of interest.

Author Contributions

K.N. and B.B. conceived the experiment and designed the patterns. B.B., Y.U., and Y.H. did the experimental work. P.R. and M.R. conceived the simulations. P.R. performed the simulations. K.N., P.R., and Y.H. wrote this work. K.N., I.N., and M.R. supervised the work. All authors reviewed the work.

Data Availability Statement

The data that support the findings of this study are available from the corresponding author upon reasonable request.

Keywords

liquid crystals, photonics, photopatterning, soft matter, waveguides

Received: August 13, 2024
Revised: October 14, 2024
Published online: November 6, 2024

[1] S. Y. Siew, B. Li, F. Gao, H. Y. Zheng, W. Zhang, P. Guo, S. W. Xie, A. Song, B. Dong, L. W. Luo, C. Li, X. Luo, G.-Q. Lo, *J. Lightwave Technol.* **2021**, *39*, 4374.
[2] H. Ma, A. K.-Y. Jen, L. R. Dalton, *Adv. Mater.* **2002**, *14*, 1339.
[3] S. Kang, G. Dong, J. Qiu, Z. Yang, *Opt. Mater.: X* **2020**, *6*, 100051.
[4] D. C. Zografopoulos, R. Asquini, E. E. Kriezis, A. D'Alessandro, R. Beccherelli, *Lab Chip* **2012**, *12*, 3598.
[5] F. Du, Y. Q. Lu, S. T. Wu, *Appl. Phys. Lett.* **2004**, *85*, 2181.
[6] S. Ertman, A. K. Srivastava, V. G. Chigrinov, M. S. Chychłowski, T. R. Woliński, *Liq. Cryst.* **2012**, *40*, 1.
[7] S. Ertman, T. R. Wolinski, D. Pysz, R. Buczynski, E. Nowinowski-Kruszelnicki, R. Dabrowski, *Opt. Express* **2009**, *17*, 19298.
[8] B. Maune, R. Lawson, G. Gunn, A. Scherer, L. Dalton, *Appl. Phys. Lett.* **2003**, *83*, 4689.
[9] W. De Cort, J. Beeckman, R. James, F. A. Fernández, R. Baets, K. Neyts, *Opt. Lett.* **2009**, *34*, 2054.
[10] V. G. Chigrinov, *Crystals* **2013**, *3*, 149.
[11] A. d'Alessandro, B. Bellini, D. Donisi, R. Beccherelli, R. Asquini, *IEEE J. Quantum Electron.* **2006**, *42*, 1084.
[12] U. S. Tripathi, V. Rastogi, *J. Lightwave Technol.* **2020**, *38*, 4045.
[13] X. Hutsebaut, C. Cambournac, M. Haelterman, A. Adamski, K. Neyts, *Opt. Commun.* **2004**, *233*, 211.
[14] J. Beeckman, K. Neyts, M. Haelterman, *J. Opt. A: Pure Appl. Opt.* **2006**, *8*, 214.
[15] J. F. Henninot, M. Debailleul, F. Derrien, M. Warenghem, *J. Opt. A: Pure Appl. Opt.* **2003**, *5*, 250.
[16] V. G. Chigrinov, V. M. Kozenkov, H. S. Kwok, in *Photoalignment of Liquid Crystalline Materials: Physics and Applications*, John Wiley & Sons, Chichester, UK **2008**.
[17] T. Wei, P. Chen, M. J. Tang, G. X. Wu, Z. X. Chen, Z. X. Shen, S. J. Ge, F. Xu, W. Hu, Y. Q. Lu, *Adv. Opt. Mater.* **2020**, *8*, 201902033.
[18] B. Berteloot, I. Nys, X. Xue, J. Beeckman, K. Neyts, *J. Mol. Liq.* **2021**, *337*, 116238.
[19] P. Ropač, **2024**, https://zenodo.org/records/12205418.
[20] I. Nys, P. Ropač, B. Berteloot, M. Ravnik, K. Neyts, *J. Mol. Liq.* **2023**, *383*, 122062.
[21] J. Li, C. H. Wen, S. Gauza, R. Lu, S. T. Wu, *J. Disp. Technol.* **2005**, *1*, 51.
[22] A. F. Oskooi, D. Roundy, M. Ibanescu, P. Bermel, J. D. Joannopoulos, S. G. Johnson, *Comput. Phys. Commun.* **2010**, *181*, 687.
[23] J. Sun, A. K. Srivastava, L. Wang, V. G. Chigrinov, H. S. Kwok, *Opt. Lett.* **2013**, *38*, 2342.
[24] B. Berteloot, I. Nys, G. Poy, J. Beeckman, K. Neyts, *Soft Matter* **2020**, *16*, 4999.
[25] L. De Sio, D. E. Roberts, Z. Liao, S. Nersisyan, O. Uskova, L. Wickboldt, N. Tabiryan, D. M. Steeves, B. R. Kimball, *Opt. Express* **2016**, *24*, 18297.

© 2024 The Author(s). Advanced Optical Materials published by Wiley-VCH GmbH

21951071, 2025, 4, Downloaded from https://advanced.onlinelibrary.wiley.com/doi/10.1002/adom.202402174 by Universiteitsbibliotheek Gent, Wiley Online Library on [18/03/2025]. See the Terms and Conditions (https://onlinelibrary.wiley.com/terms-and-conditions) on Wiley Online Library for rules of use; OA articles are governed by the applicable Creative Commons License